Increased Stress Along the Sumpur and Northern Sianok Segments of Sumatran Fault Due to the 25 February 2022 $M_{\rm w}$ 6.1 Pasaman, Indonesia, Earthquake



Endra Gunawan^{1,2}, Nanang T. Puspito^{1,2}, Andri Dian Nugraha^{1,2}, Sri Widiyantoro^{1,2}, Risya Fauziyyah³, Medina Apriani³, Nuraini Rahma Hanifa⁴, Ekbal Hussain^{*5}, Bayu Triyogo Widyantoro⁶, and Sidik Tri Wibowo⁶

Abstract

On 25 February 2022, a destructive $M_{
m w}$ 6.1 earthquake struck western Sumatra in the early hours of the morning. The earthquake shaking was focused around the Pasaman Regency and resulted in 25 fatalities. Coseismic displacements were recorded by an existing network of Global Navigation Satellite System (GNSS) sensors managed by the Geospatial Information Agency of Indonesia. The GNSS data show a maximum of 2.0 cm of displacement with a right-lateral sense of motion across a northwest-southeast-trending fault. An investigation into the responsible fault producing the earthquake is performed through a series of coseismic slip inversions on a rectangular fault plane, comparing two fault models: (a) a fault segment that is an extension of the already identified Sianok segment of the Sumatran fault zone, and (b) the recently identified Talamau segment. The maximum slip of 14 cm occurred at 4 km depth, 13 km away from the epicenter. The mainshock is associated to a seismic moment of 1.58 × 10²⁵ N·m, or equivalent to $M_{\rm w}$ 6.1. Our results indicate increased stress along the Sumpur segment and the northern Sianok segment. With no historical earthquakes reported along the Sumpur and northern Sianok segments since 1892, our analysis using a scaling relationship between fault length and earthquake magnitude indicates that a rupture in these areas could potentially generate an earthquake with a magnitude of 6.7.

Cite this article as Gunawan, E., N. T. Puspito, A. D. Nugraha, S. Widiyantoro, R. Fauziyyah, M. Apriani, N. R. Hanifa, E. Hussain, B. T. Widyantoro, and S. T. Wibowo (2025). Increased Stress Along the Sumpur and Northern Sianok Segments of Sumatran Fault Due to the 25 February 2022 $M_{\rm w}$ 6.1 Pasaman, Indonesia, Earthquake, Seismol. Res. Lett. XX, 1–10, doi: 10.1785/0220240476.

Supplemental Material

Introduction

Accurate detection of fault slip and deformation is crucial for understanding the full cycle of strain accumulation and release in an earthquake (Wang et al., 2012; Wright, 2016). Global Navigation Satellite Systems (GNSS) have been widely employed to study tectonic processes in various earthquake cases (e.g., Bürgmann et al., 2013; Nishimura et al., 2014; Feng et al., 2015; Larson, 2019). In these cases, the coseismic surface deformation recorded by the GNSS sensors is inverted, often assuming an elastic half-space (e.g., Tanaka et al., 2019; Gunawan, Gualandi, et al., 2024), to determine the magnitude and distribution of slip on the fault plane.

Sumatra, one of the world's most tectonically active regions, experiences frequent earthquakes due to the interplay between the dip-slip component of the Sumatra subduction zone and the strike-slip component of the Sumatran fault (McCaffrey, 2009). The Sumatran fault is a major right-lateral fault zone running for 1900 km along the entire length of the island with an average slip rate of 15–16 mm/yr (Ito et al., 2012; Bradley et al., 2017). Of

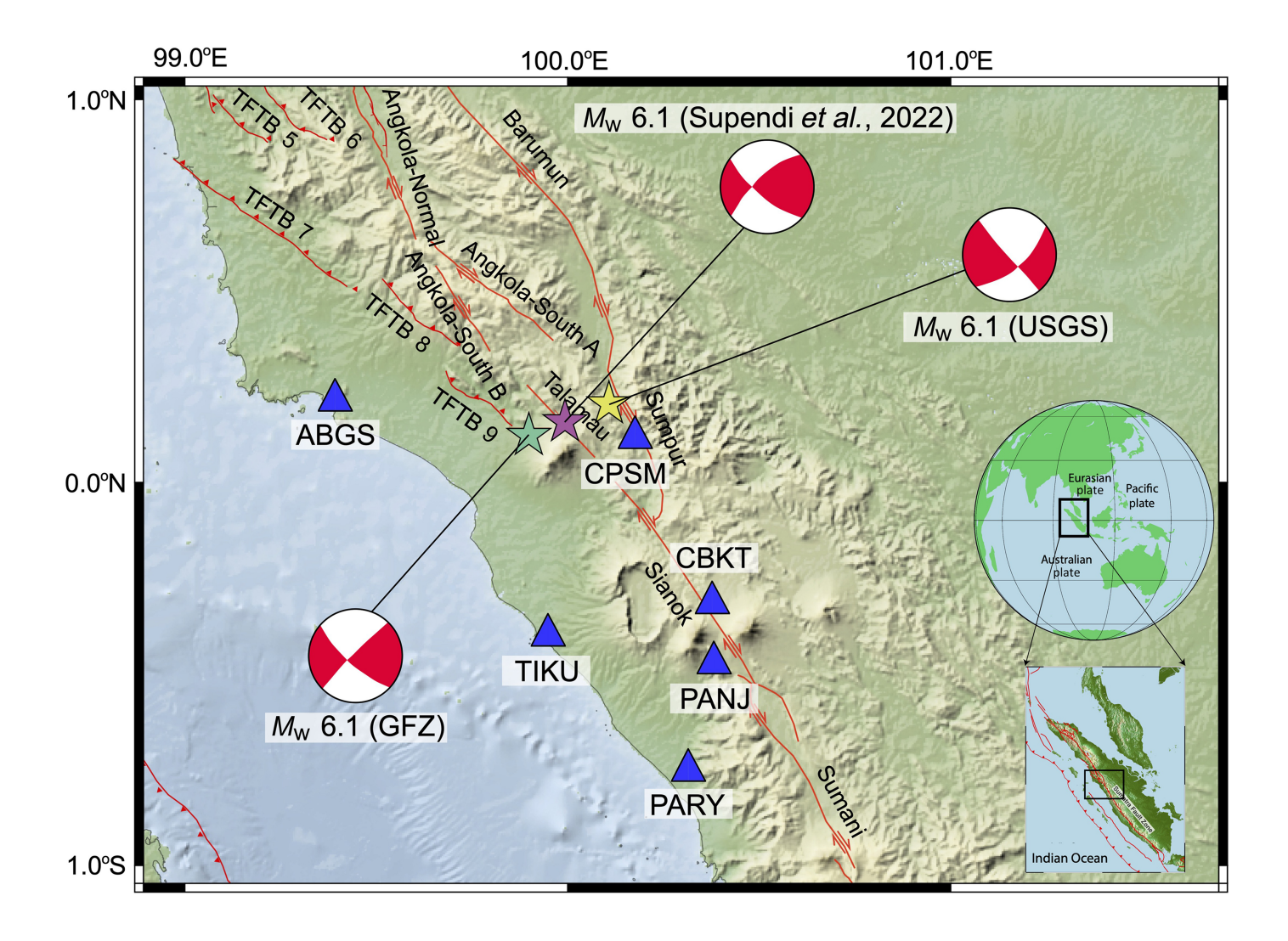
the 42 total Sumatran fault segments, which pose a threat to everyone living on the west coast of the island, seven are located in West Sumatra Province (Irsyam et al., 2020).

On 25 February 2022, at 01:39 UTC, an $M_{\rm w}$ 6.1 earthquake occurred at Pasaman, West Sumatra, Indonesia, with a shallow depth of 4 km (Supendi *et al.*, 2023). The Indonesian National

Copyright © 2025. The Authors. This is an open access article distributed under the terms of the CC-BY license, which permits unrestricted use, distribution, and reproduction in any medium, provided the original work is properly cited.

^{1.} Global Geophysics Research Group, Faculty of Mining and Petroleum Engineering, Institut Teknologi Bandung, Bandung, Indonesia, 19 https://orcid.org/0000-0002-4844-8723 (ADN); 10 https://orcid.org/0000-0002-8941-7173 (SW); 2. Research Center for Disaster Mitigation, Institut Teknologi Bandung, Bandung, Indonesia; 3. Geophysical Engineering Study Program, Faculty of Mining and Petroleum Engineering, Institut Teknologi Bandung, Bandung, Indonesia; 4. Research Center for Geological Disaster, National Research and Innovation Agency, Bandung, Indonesia, 10 https://orcid.org/0000-0002-8012-5385 (NRH); 5. British Geological Survey, Nottingham, United Kingdom, 10 https://orcid.org/0000-0001-6921-2843 (EH); 6. Geospatial Information Agency, Cibinong, Indonesia, 10 https://orcid.org/0000-0001-5117-2740 (BTW); 11 https://orcid.org/0009-0002-6816-5920 (STW)

^{*}Corresponding author: ekhuss@bgs.ac.uk



Board for Disaster Management reported 25 fatalities, at least 465 injuries, and the displacement of over 16,000 people. According to the U.S. Geological Survey (USGS) earthquake catalog, the epicenter was located northeast of Mount Talamau, positioned south of the Angkola segment, west of the Sumpur segment, and north of the Sianok segment of the seismically active Sumatran fault (Fig. 1). The hypocenter's location, not closely associated with any known Sumatran fault segments, raises intriguing questions about the fault source of the earthquake.

Supendi *et al.* (2023) conducted a relocation of the foreshock, mainshock, and aftershocks, with a total of 201 seismic events ranging in magnitude from 1.4 to 6.1. These seismic events, which included a foreshock, mainshock, and aftershocks, were recorded over the 12-day period from 25 February to 8 March 2022. The aftershocks revealed a previously unidentified section of the Sumatran fault. This newly discovered segment, which Supendi *et al.* (2023) named the Kajai fault segment, is approximately 20 km long and characterized by right-lateral strike-slip movement. The fault has a strike orientation of N132°E and a dip angle of 72° to the southwest. This fault is approximately 15 km to the west of the currently identified Sumpur segment. However, the USGS catalog suggested that

Figure 1. Tectonic setting of the study area. Locations of the Global Navigation Satellite System (GNSS) stations used in this study are shown by blue triangles. The epicenter location of the 25 February 2022 Pasaman earthquake with focal mechanisms is from the U.S. Geological Survey (USGS) catalog (yellow star), GeoForschungsZentrums (GFZ) catalog (green star), and Supendi *et al.* (2023; purple star). The solid red lines indicate the identified fault trace of the Sumatran fault based on the National Center for Earthquake Studies of Indonesia (2024). Inset shows the regional map. The color version of this figure is available only in the electronic edition.

the epicenter is located at the Sumpur segment. These two different epicenter locations raised questions about which is the responsible fault segment of the 2002 Pasaman earthquake.

This study investigates the coseismic deformation of the 25 February 2022 Pasaman earthquake using GNSS data to determine the responsible fault segment of the earthquake. We apply a Bayesian inversion model to calculate the coseismic slip using two fault model scenarios (e.g., Fukahata and Wright, 2008; Li *et al.*, 2015). We also explore the stress transfer impacts of the earthquake on nearby faults. We analyze the

Coulomb stress change to investigate the potential seismic risk along the Sumatran fault (e.g., Toda and Stein, 2003). Finally, we discuss the implications of our coseismic slip model on earthquake scaling relationships, which are often used in seismic hazard analysis.

Data and Method GPS

This study utilizes GNSS data, which is recorded as part of the Indonesia Continuously Operating Reference Station (Ina-CORS; Gunawan et al., 2022), and provided by the Geospatial Information Agency of Indonesia, and the Sumatran Global Positioning System (GPS) Array (SuGAr), which is maintained by the Earth Observatory of Singapore and National Research and Innovation Agency of Indonesia (BRIN; e.g., Feng et al., 2015). There are three GNSS stations from the Ina-CORS network available in the region; in Bukittinggi (CBKT), West Pasaman (CPSM), and Padang Panjang (PANJ). Meanwhile, another three GNSS data from SuGAR network are in West Pasaman (ABGS), Agam (TIKU), and Padang Pariaman (PARY). The location of these GNSS stations is shown in Figure 1.

GNSS data from the Ina-CORS network were processed using GAMIT (Herring et al., 2010a,b), and daily solutions were obtained through a three-stage process (e.g., Gunawan et al., 2022). First, daily positions were estimated using atmospheric zenith delays and loose constraints at each station, incorporating prior GNSS phase observations with fixed orbit and earth-orientation parameters. Next, these positions and their covariance were combined with global GNSS solutions from Massachusetts Institute of Technology (MIT)'s International GNSS Service (IGS) processing. The loosely constrained solution was then transformed into a well-constrained reference frame by minimizing position and velocity differences between selected stations and their prior IGS14-defined values within the International Terrestrial Reference Frame (ITRF) 2014 (Altamimi et al., 2016). The final position time series was subsequently estimated.

Meanwhile, the GNSS data from the SuGAr network are downloaded in a RINEX format (see Data and Resources), which is collected over a 30 s interval. This data are processed using the GipsyX software (Bertiger et al., 2020), by employing a precise point positioning technique to estimate the daily solutions of the GNSS data (Gunawan et al., 2023). The Jet Propulsion Laboratory's reanalysis of the final set of the IGS 2014 (IGS14) orbit and clock product was utilized to actualize the ITRF2014 reference (Altamimi et al., 2016). Five iterations of fiducial-free processing were also employed, with the elevation cutoff angle set at 15°. In addition, the ocean-loading parameters of the GOT4.8 model obtained from the Onsala Space Observatory were also used.

Fault-plane model

The 2022 Pasaman earthquake epicenter occurred in a region with no previously identified segment of the Sumatran fault. Thus, we investigate two possible fault-plane models to estimate the coseismic slip of the mainshock. The first fault-plane model, named model 1, built by extending the Sianok segment of the Sumatran fault (Fig. 1) to the northwest direction toward the epicenter. Our approach is based on the assumption that the mainshock occurred along the Sianok segment. We construct a fault with length of 103 km, width of 32 km, strike of 327°, and dip of 90° (Fig. 2). Along length, we divide the fault into nine subfaults, in which length is varied from 5 to 25 km. Along width, we divide the fault into four subfaults, in which the width is 8 km.

The second fault-plane model, named model 2, is constructed using the information from the USGS catalog. We construct a fault with strike 319°, dip of 90°, length of 20 km, and depth of up to 32 km (Fig. 3). Fault length is obtained based on the earthquake scaling relationship proposed by Gunawan (2021). In this model, we divided the fault into subfaults with size of 4 km in length and 8 km in width.

Coseismic slip modeling

Using the daily solutions data, we calculate the coseismic displacement by subtracting the average displacement from five-day intervals after—with before—the mainshock. Our calculation involves three components of the GNSS data: the easting, northing, and vertical components. The standard deviation is obtained by averaging the error of the daily solutions data at each station.

We estimated the coseismic slip distribution using a Bayesian inversion approach developed by Yabuki and Matsu'ura (1992), based on observed coseismic displacements. The slip is computed using the equation: $s(m) = (d - Gm)^T E^{-1} (d - Gm) + \alpha^2 m^T Lm$. In this formulation, G represents the Green's function derived from an elastic dislocation model (Okada, 1992) with a Poisson's ratio of 0.25, E denotes the measurement variance-covariance matrix, α^2 is a hyperparameter, and E is a Laplacian smoothing matrix. We determined the optimal hyperparameter using Akaike's Bayesian information criterion (ABIC; e.g., Gunawan, Gualandi, et al., 2024). In our procedure, diagonal elements of the covariance matrix are also calculated.

Processing ResultCoseismic displacements

Our results indicate that the largest coseismic displacement was recorded at the CPSM station, with a displacement of 2.0 cm to the east. Similarly, the CBKT station also experienced displacement in the same direction, albeit with a smaller magnitude of 0.4 cm. In contrast, three stations (ABGS, TIKU, and PARY) exhibited coseismic displacements toward the northwest, with magnitudes of 0.5, 0.4, and 0.2 cm, respectively. The smallest displacement, measuring 0.1 cm, was directed

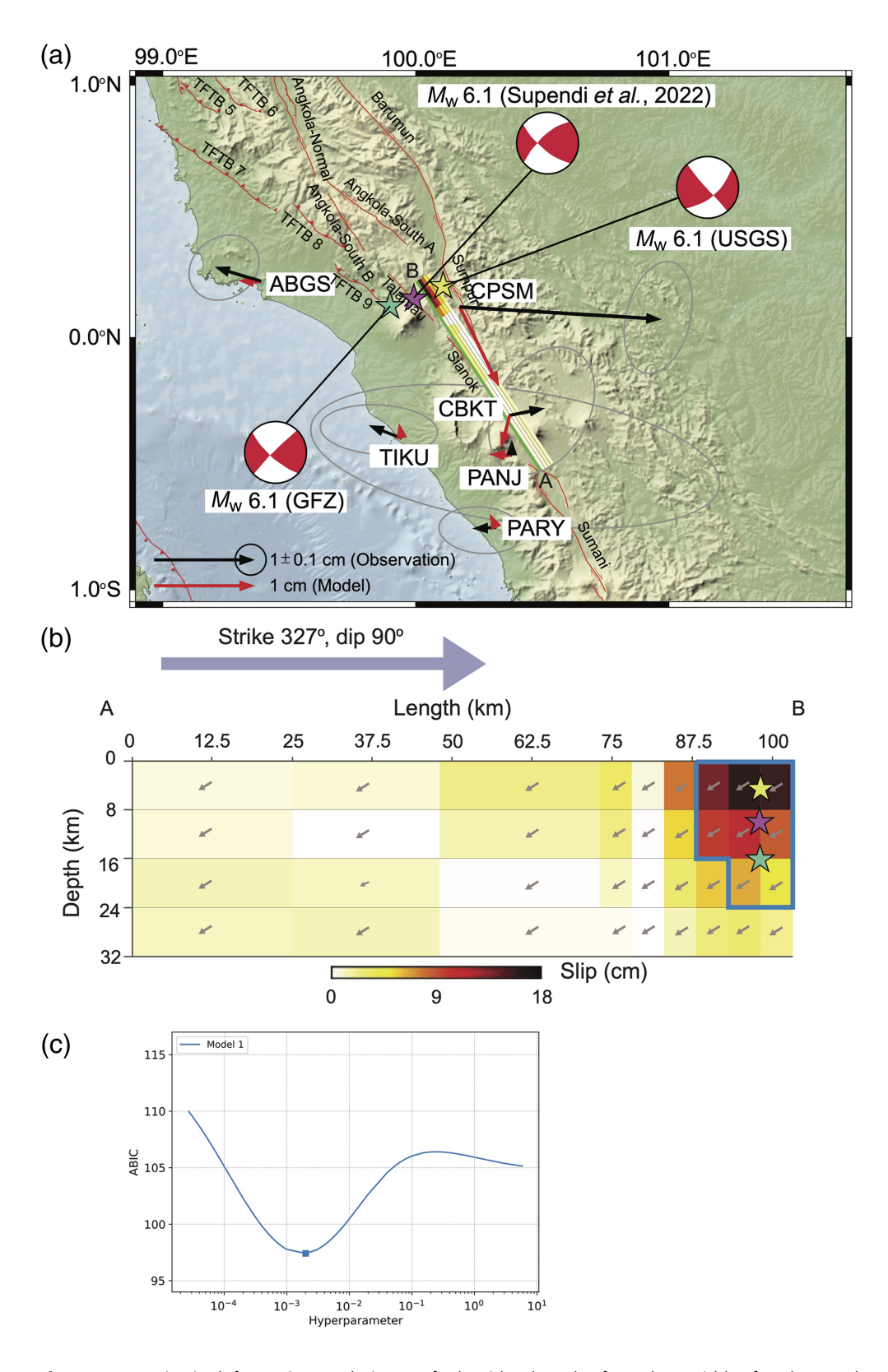


Figure 2. Coseismic deformation analysis on a fault with a length of 103 km, width of 32 km, and fault strike and dip of 327° and 90°, respectively (model 1). (a) Coseismic displacements of the 2022 Pasaman earthquake, which is shown by black vectors. Red vectors indicate the modeled coseismic displacements. (b) The inferred coseismic slip of the 2022 Pasaman earthquake using a fault geometry of model 1. Gray vectors indicate the rake direction. Slip within the blue polygons indicates where the estimated uncertainty is lower than the absolute value of the predicted slip. (c) Hyperparameter as a function of Akaike's Bayesian information criterion (ABIC) with best-fit parameter shown by the blue square (see Fig. 1 for a detailed description of the figure legend). The color version of this figure is available only in the electronic edition.

toward the north and was recorded at the PANJ station. The spatial patterns of these displacements are visually represented in Figures 2 and 3.

Coseismic slip

Coseismic slip is estimated by employing the α^2 hyperparameter for which the ABIC is minimum. The best-fit ABIC parameter that is used for final model in model 1 is 97.42 (Fig. 2), whereas in model 2 is 95.43 (Fig. 3). Inverted GPS data on model 1 show that the maximum slip is around 16 cm, which is focused at 4 km deep, located approximately 9 km from Pasaman earthquake epicenter (Fig. 2). In model 2, the inversion data indicate that the maximum slip is about 14 cm at the same depth as the previous model, located 13 km away from the epicenter (Fig. 3). The region where the estimated slip uncertainty is lower than the absolute value of the predicted slip is shown in Figures 2 and 3.

The misfit between coseismic displacement data and inversion data is calculated using the mean absolute error (MAE), defined as follows: $MAE=1/n\sum_{i=1,n}|data_i|$ $-\text{model}_i$, in which n is the total number of data consisting of east, north, and up components. We found that model 1 had a misfit of 4 mm, whereas model 2 had a smaller misfit of 2 mm. Calculating the seismic moment from the coseismic slip result, we found that model 1 corresponds to $7.26 \times 10^{24} \text{ N} \cdot \text{m}$, equivalent to $M_{\rm w}$ 5.8 when assuming a shear modulus of 33 GPa. Meanwhile, model 2 is associated with $1.58 \times 10^{25} \text{ N} \cdot \text{m}$

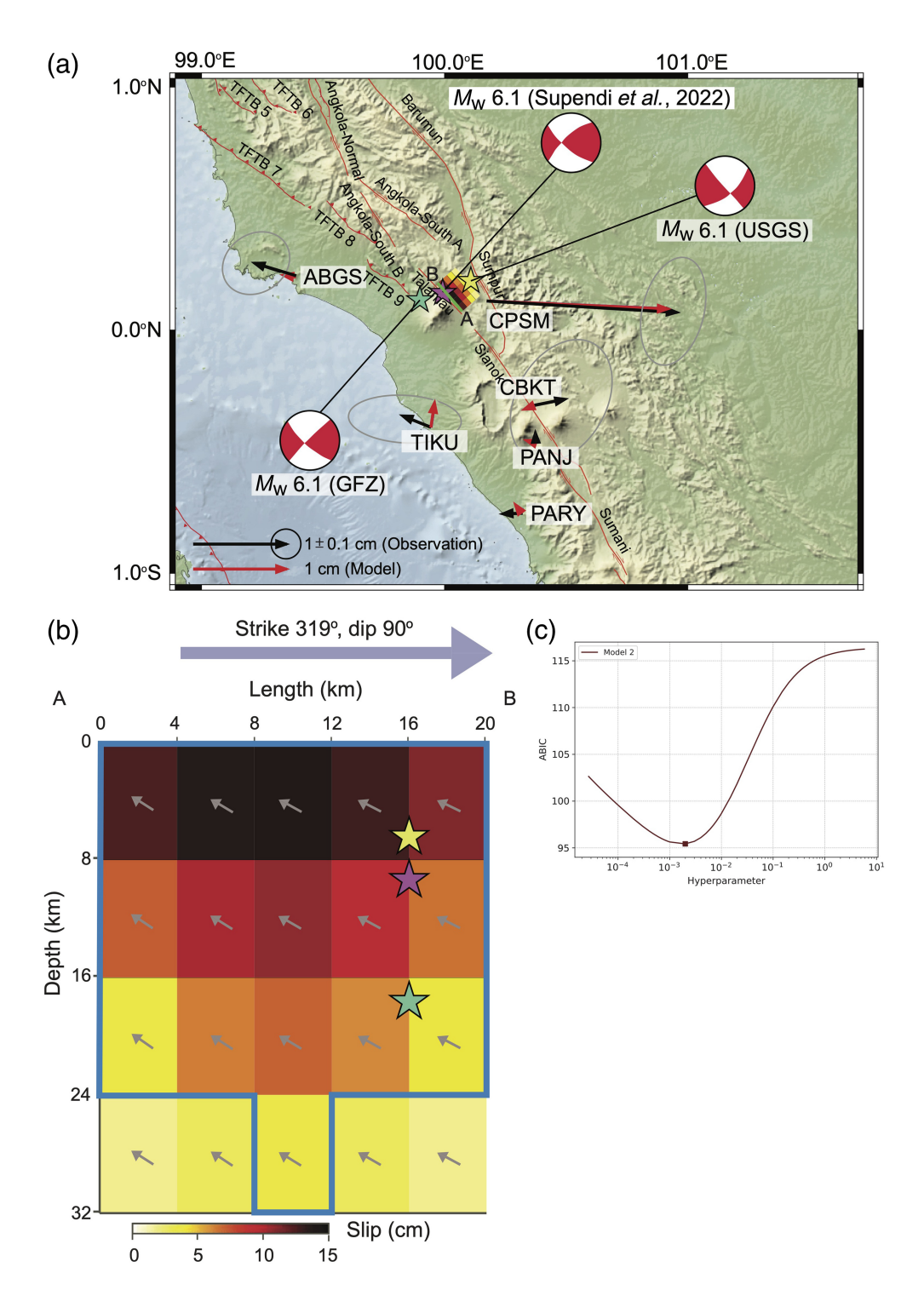


Figure 3. Coseismic deformation analysis on a fault with a length of 20 km, width of 32 km, and fault strike and dip of 319° and 90°, respectively (model 2). (a) Coseismic displacements of the 2022 Pasaman earthquake, which is shown by black vectors. Red vectors indicate the modeled coseismic displacements. (b) The inferred coseismic slip of the 2022 Pasaman earthquake using a fault geometry of model 2. Gray vectors indicate the rake direction. Slip within the blue polygons indicates where the estimated uncertainty is lower than the absolute value of the predicted slip. (c) Hyperparameter as a function of ABIC with best-fit parameter shown by the red square (see Fig. 1 for a detailed description of the figure legend). The color version of this figure is available only in the electronic edition.

or equivalent to $M_{\rm w}$ 6.1, if we use the same shear modulus value.

DiscussionIdentification of the ruptured fault segment

The epicenter location from USGS catalog showed that the earthquake may have occurred along Sumpur segment (Fig. 1). If this is true, then the coseismic displacements at CPSM station, which is located in the western part of the Sumpur segment, should exhibit northwest motion. Instead, the coseismic displacement at this station has a southeast direction, suggesting that this station is located on the eastern part of the fault.

Following Supendi et al. (2023), the epicenter of the 2022 Pasaman earthquake occurred in a previously unknown fault segment, located between the Angkola segment and the Sianok segment. By having the epicenter at this location, the coseismic displacements at the right part of the fault segment should exhibit a southeast direction, which is what we see in the coseismic displacements data at CPSM. Thus, we conclude that the mainshock did not occur along the Sumpur segment; instead, it occurred on an unknown fault segment between the Angkola segment and the Sianok segment, validating the inferences of Supendi et al. (2023).

The National Center for Earthquake Studies (2024) defined this unknown fault segment as the Talamau segment (Fig. 1). In our model 1, although we include the Sinaok segment, our result showed that maximum slip occurred near the epicenter,

closer to the Talamau segment. Nonetheless, with the inclusion of Sianok segment in the process, model 1 failed to predict GNSS station observations closest to the epicenter, CPSM (Fig. 2). On the other hand, model 2 successfully predicts the coseismic displacements at CPSM by modeling only using a fault with a length of 20 km. In terms of error, model 2 also produces a smaller MAE than model 1. For these reasons, we consider model 2 as our preferred model and use it for further analysis.

Model 2 suggests that coseismic slip extends to a depth of approximately 24 km. In line with this, Prawirodirdjo *et al.* (2000) investigated the fault slip rate and locking depth along the Sumatran fault using historical triangulation and GNSS data. They found that the locking depth of the Sianok segment is also around 24 km. Our coseismic slip results are therefore consistent with their earlier estimates.

We compare our preferred coseismic slip model 2 with the coseismic slip model from the arrival-time dataset by Supendi et al. (2023). Their study showed that aftershock distributed extending ~20 km northwest–southeast parallel to the Sumatran fault, which they named the Kajai segment. The location of Kajai and Talamau segments is identical. Thus, both segments are similar, only differing in naming. Finally, our GNSS-based investigation of the 2022 Pasaman earthquake rupture along Talamau segment is supported by the seismic investigation.

Potential seismic hazard along the Sumatran fault

Aftershocks can be triggered by the stress generated from preceding mainshocks, with their spatial patterns being particularly challenging to forecast. Although shear stress change provides a better measure of potential earthquake triggering, Coulomb failure stress remains one of the most widely used criteria to explain the spatial distribution of aftershocks (e.g., DeVries *et al.*, 2018).

The friction coefficient of rocks exhibits a strong dependence on normal stress at typical crustal depths. For Coulomb stress calculations, the typical assumption is that frictional resistance is linearly proportional to the effective normal stress (King et al., 1994). Barbot (2024) suggests that there may be a time-dependent, nonlinear relationship between friction and normal stress and attributes this to heterogeneities in the fault geology and asperity distribution. However, in this study, we do not have geological information and produce slip distribution to the level of detail required to disentangle this effect, and therefore, we maintain the assumption of a linear relationship between friction and normal stress.

The Coulomb stress change imparted by the 2022 Pasaman earthquake rupture could be used to determine if a neighboring fault is brought closer to failure and, thus, provide information on the possible region where earthquakes may occur in the future (e.g., Toda *et al.*, 2011; Gunawan *et al.*, 2022).

In this study, we compute the Coulomb stress change (Δ CFF) using the equation Δ CFF = $\Delta \tau + \mu^{'} \Delta \sigma$, in which

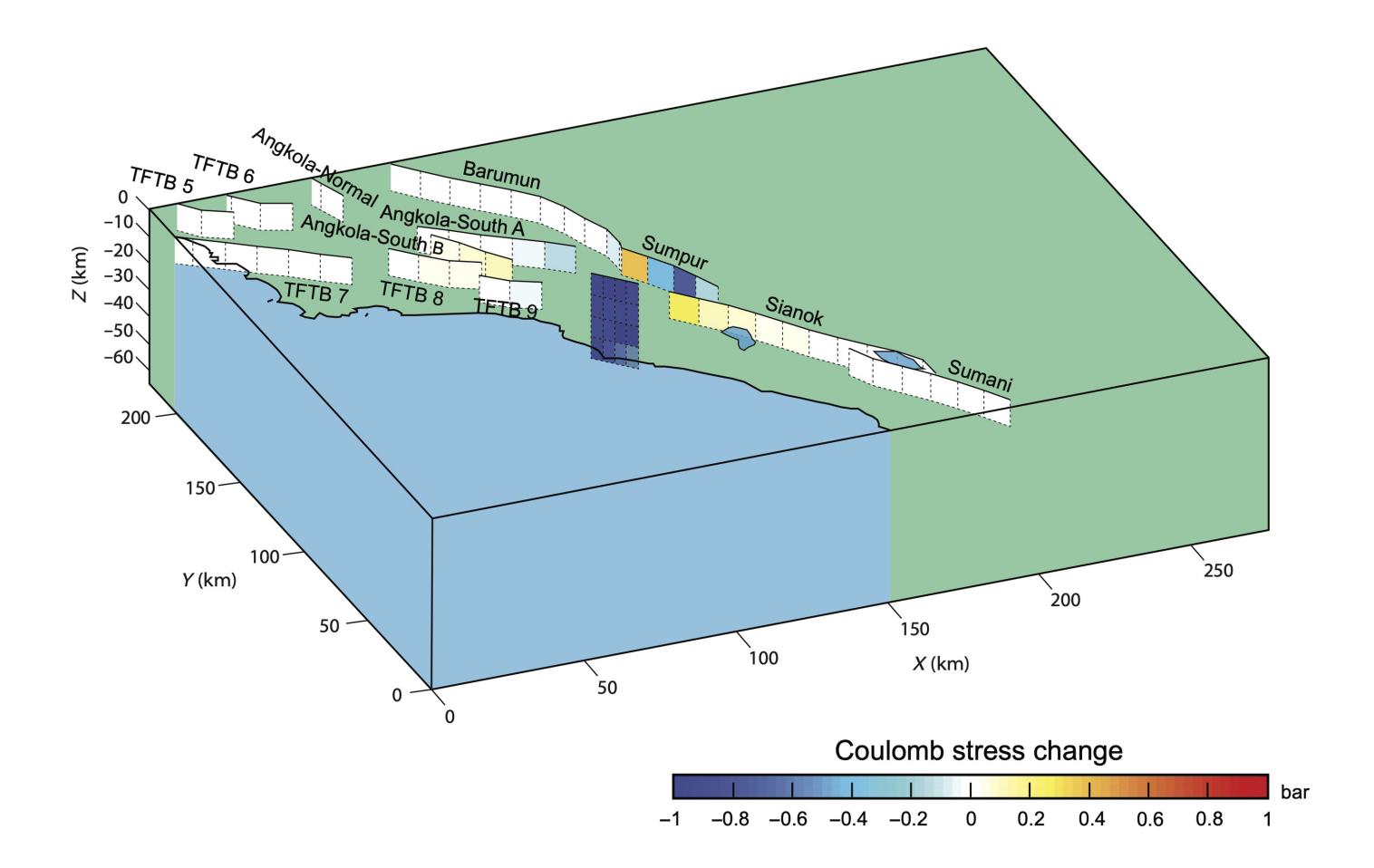
 $\Delta \tau$ represents the change in shear stress on a specific fault plane (with positive values indicating promotion of slip along the receiver fault), μ' denotes the effective friction coefficient on the receiver fault, and $\Delta \sigma$ represents the change in normal stress acting on the fault plane (for which positive values signify unclamping or reduction in normal stress). This methodology aligns with approaches outlined in previous research (e.g., King *et al.*, 1994; Hardebeck *et al.*, 1998; Lin and Stein, 2004; Toda *et al.*, 2005). In our calculation, we used a Poisson ratio of 0.25, Young's modulus of 8×10^5 bar, and a friction coefficient of 0.8.

To see the variation of stress along the receiver faults consisting of the Barumun, Sumpur, Angkola, Sianok, and Sumani segments, a fault model was created from the coseismic slip model 2. Our result suggests that the $M_{\rm w}$ 6.1 2022 Pasaman earthquake increased stress along the Sumpur segment and the northern Sianok segment by approximately 0.4 and 0.3 bar, bringing these segments closer to failure (Fig. 4). Hurukawa *et al.* (2014) reported that no historical earthquake has been reported along the Sumpur and northern Sianok segments since at least 1892. If these segments rupture, it may generate an earthquake with a magnitude of 6.7 (National Center for Earthquake Studies, 2024).

Meade et al. (2017) suggest that maximum shear stress and the magnitudes of the second and third invariants of the stress tensor are higher by 10% in explaining aftershocks compared to Coulomb stress. Regardless, Coulomb stress still satisfactorily explains seismicity in various cases, such as the Rangely oil field in Colorado (Byrne et al., 2020), the 2016 Mie offshore earthquake in Japan (Yoshida et al., 2020), the 2020 Samos earthquake (Lentas et al., 2022), the 2022 Chihshang earthquake (Murase et al., 2025), the 2021 Fukushima earthquake (Zhang et al., 2023), and many other studies. Nonetheless, further investigation is needed to explore the role of maximum shear stress and the magnitudes of the second and third invariants of the stress tensor in the context of the 2022 Pasaman earthquake.

Implication of coseismic slip model to earthquake scaling relationship

Empirical relationships between fault geometry and earthquake magnitude (e.g., Wells and Coppersmith, 1994) have been widely used in earthquake magnitude estimation in seismic hazard analysis (e.g., Irsyam et al., 2020). We use the earthquake scaling relationships for the tectonic region of Indonesia (Gunawan, 2021) for strike-slip faulting regimes, which proposed a relationship between fault length and earthquake magnitude. We further analyze this empirical function with the case of the 2022 Pasaman earthquake and five other large earthquakes on the Sumatran fault based on the work of Gunawan et al. (2018), Gunawan et al. (2020), and Salman et al. (2020). Those major earthquakes are the 2007 $M_{\rm w}$ 6.3 Sianok earthquake at the southern segment, 2007 $M_{\rm w}$ 6.4 Sumani earthquake, 2009



 $M_{\rm w}$ 6.6 Dikit earthquake (Salman *et al.*, 2020), 2013 $M_{\rm w}$ 6.1 Aceh earthquake, and 2016 $M_{\rm w}$ 6.5 Aceh earthquake. Another major strike-slip earthquake, that is the 2018 $M_{\rm w}$ 7.6 Palu Donggala earthquake (Socquet *et al.*, 2019), was also used as a comparison. Figure 5 shows the comparison between parameters of those earthquakes (magnitude and fault length) with the earthquake scaling relationship model of Gunawan (2021).

By comparing the earthquake scaling relationship model and these major strike-slip earthquakes, we show that the 2022 Pasaman earthquake follows the empirical function satisfactorily (Fig. 5). The fault length of model 1 did not follow the earthquake scaling relationship, resulting in a poor prediction of the GNSS displacements. Thus, estimating an earthquake magnitude from fault length information can be a simple but rapid way to estimate future earthquake potential.

Marliyani *et al.* (2016) showed that the Cimandiri fault, in western Java, Indonesia, consists of six segments, where each segment may generate earthquakes between 6.5 and 6.9. However, the case of the 2018 $M_{\rm w}$ 7.6 Palu Donggala earthquake showed that crustal earthquakes in Indonesia could reach up to $M_{\rm w}$ 7.6. Thus, assuming a similar case to the Cimandiri fault, it could reach a magnitude of up to $M_{\rm w}$ 7.3. The 2022 Cianjur earthquake in western Java showed that it did not necessarily need a magnitude 7 class earthquake to be devastating (Gunawan, Hanifa, *et al.*, 2024). An $M_{\rm w}$ 5.6 is enough to generate damage to ~56,548 buildings, and more

Figure 4. Stress imparted by the fault rupture of model 2 to the surrounding active faults. Except for the Talamau segment, the top and bottom depths of the active faults are set to 0 and 10 km, respectively. The color version of this figure is available only in the electronic edition.

than 300 fatalities. In such cases, the background seismicity is key to conducting seismic hazard assessment. However, defining the minimum magnitude is a challenge that needs to be considered based on the completeness of the recorded seismicity in each region.

Conclusion

This study has investigated the responsible fault segment of the 2022 Pasaman earthquake using GNSS data. We found that the mainshock ruptured a newly recognized segment of the Sumatran fault named by the National Center for Earthquake Studies as the Talamau segment. The maximum slip of 14 cm in our best-fit model occurred at 4 km depth, 13 km away from the epicenter. Assuming the shear modulus of 33 GPa, we found that the earthquake was associated with a seismic moment of $1.58 \times 10^{25}~{\rm N} \cdot {\rm m}$, or equivalent to $M_{\rm w}$ 6.1. We also explore the impact of the earthquake on nearby faults. Using the Coulomb stress change investigation, we found that the 2022 $M_{\rm w}$ 6.1 Pasaman earthquake increased stress along the

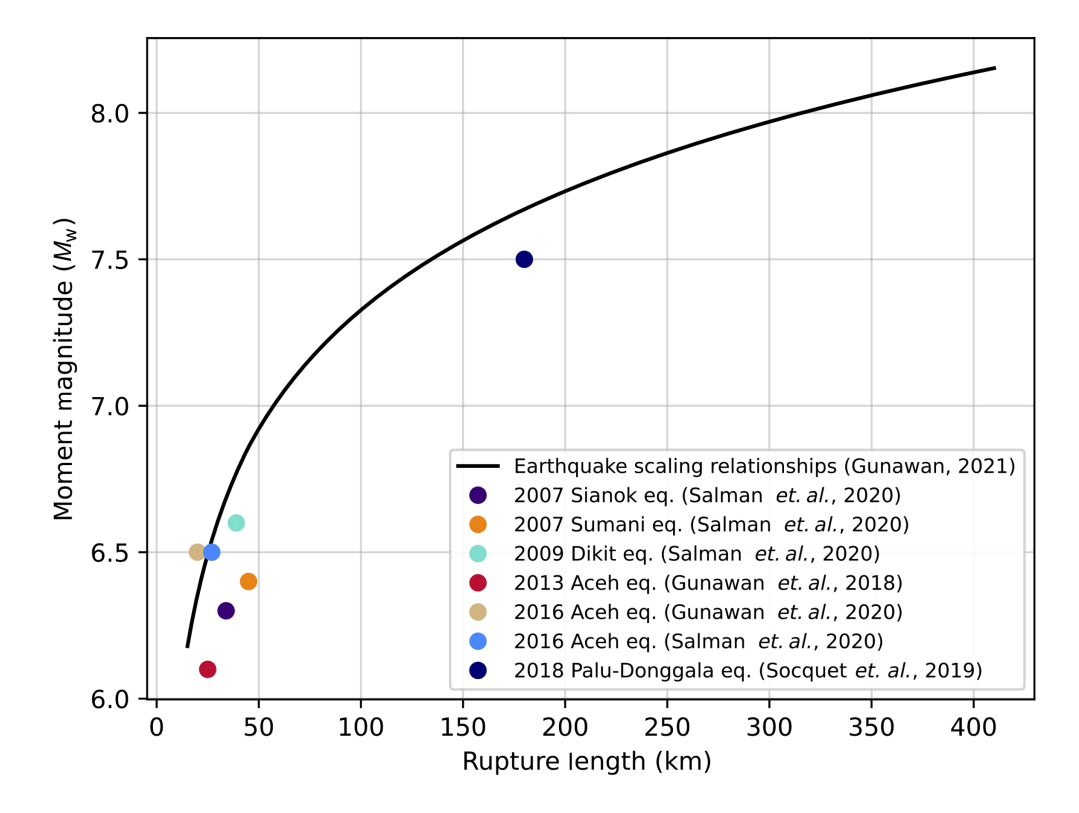


Figure 5. Rupture length as a function of moment magnitude. A solid black line indicates the earthquake scaling relationship for rupture length and moment magnitude based on Gunawan (2021). Color dots represent various earthquake cases from Socquet *et al.* (2019), Salman *et al.* (2020), and Gunawan *et al.* (2018, 2020). The color version of this figure is available only in the electronic edition.

Sumpur and the northern Sianok segments by approximately 0.4 and 0.3 bar bringing these closer to failure. Given that no historical earthquake has been reported along Sumpur and northern Sianok segments since at least 1892, an earthquake with a magnitude of 6.7 may occur if these segments were to rupture. Finally, we show that the 2022 Pasaman earthquake follows the empirical earthquake scaling relationship between fault length and earthquake magnitude for active regions in Indonesia developed by Gunawan (2021). Thus, estimating an earthquake magnitude from fault length information is a simple but rapid way of estimating future earthquake potential on faults with otherwise little information.

Data and Resources

The data and materials used and/or analyzed during the current study are available from the corresponding author on reasonable request. The ocean-loading parameters were obtained from the Onsala Space Observatory (http://holt.oso.chalmers.se/loading/, last accessed September 2024). Earthquake focal mechanisms were taken from the U.S. Geological Survey (USGS) catalog (https://earthquake.usgs.gov/earthquakes/eventpage/us6000gzyg/executive, last accessed September 2024) and GeoForschungsZentrums (GFZ) catalog (https://geofon.gfz.de/old/eqinfo/event.php?id=gfz2022dwpy, last accessed September 2024). The information about the Earth Observatory of Singapore is available at ftp://ftp.earthobservatory.sg/SugarData/ (last accessed

October 2024). The supplemental material includes a description of the inversion procedure, the Global Navigation Satellite System (GNSS) data used in the study, and a summary of the slip distribution model 2.

Declaration of Competing Interests

The authors acknowledge that there are no conflicts of interest recorded.

Acknowledgments

The authors thank two anonymous reviewers, Romain Jolivet and Editor-in-Chief Allison Bent, for their critical comments and constructive suggestions, which help improve the quality of this article. This study is supported by the 2025 Excellent Research of Institut Teknologi Bandung, 2024 the Research and Innovation for Advanced Indonesia program supported by National Research Innovation Agency of Indonesia (BRIN) and Indonesia

Endowment Fund for Education Agency (LPDP), and the Center for Excellence Research and Research Centers (RU3P; Riset Unggulan Pusat dan Pusat Penelitian) of Institut Teknologi Bandung. Ekbal Hussain is supported by the British Geological Survey International NC programme "Geoscience to tackle Global Environmental Challenges," NE/X006255/1. Ekbal Hussain publishes with permission from the Executive Director of the British Geological Survey. Figures were generated using the Generic Mapping Tools (GMT) software (Wessel *et al.*, 2019).

References

Altamimi, Z., P. Rebischung, L. Métivier, and X. Collilieux (2016). ITRF2014: A new release of the International Terrestrial Reference Frame modeling nonlinear station motions, *J. Geophys. Res.* **121**, no. 8, 6109–6131.

Barbot, S. (2024). Transient and steady-state friction in non-isobaric conditions, *Geochem. Geophys. Geosys.* **25**, no. 2, e2023GC011279, doi: 10.1029/2023GC011279.

Bertiger, W., Y. Bar-Sever, A. Dorsey, B. Haines, N. Harvey, D. Hemberger, M. Heflin, W. Lu, M. Miller, A. W. Moore, and D. Murphy (2020). GipsyX/RTGx, a new tool set for space geodetic operations and research, *Adv. Space Res.* **66**, no. 3, 469–489.

Bradley, K. E., L. Feng, E. M. Hill, D. H. Natawidjaja, and K. Sieh (2017). Implications of the diffuse deformation of the Indian

- Ocean lithosphere for slip partitioning of oblique plate convergence in Sumatra, *J. Geophys. Res.* **122**, no. 1, 572–591.
- Bürgmann, R., W. Thatcher, and M. E. Bickford (2013). Space geodesy: A revolution in crustal deformation measurements of tectonic processes, *Geol. Soc. Am. Spec. Pap.* **500**, 397–430.
- Byrne, H., J. A. Silva, A. Plesch, R. Juanes, and J. H. Shaw (2020). The groundbreaking experiment in earthquake control at Rangely, Colorado, revisited, *Geophys. Res. Lett.* **47**, no. 11, e2020GL088257, doi: 10.1029/2020GL088257.
- DeVries, P. M., F. Viégas, M. Wattenberg, and B. J. Meade (2018). Deep learning of aftershock patterns following large earthquakes, *Nature* **560**, no. 7720, 632–634.
- Feng, L., E. M. Hill, P. Banerjee, I. Hermawan, L. L. Tsang, D. H. Natawidjaja, B. W. Suwargadi, and K. Sieh (2015). A unified GPS-based earthquake catalog for the Sumatran plate boundary between 2002 and 2013, J. Geophys. Res. 120, no. 5, 3566–3598.
- Fukahata, Y., and T. J. Wright (2008). A non-linear geodetic data inversion using ABIC for slip distribution on a fault with an unknown dip angle, *Geophys. J. Int.* **173**, no. 2, 353–364.
- Gunawan, E. (2021). An assessment of earthquake scaling relationships for crustal earthquakes in Indonesia, *Seismol. Res. Lett.* **92,** no. 4, 2490–2497, doi: 10.1785/0220200267.
- Gunawan, E., R. Amey, J. Elliott, S. Widiyantoro, N. T. Puspito, N. R. Hanifa, Syamsuddin, and E. Hussain (2023). Coseismic deformation of the 19 August 2018 Mw 7.2 Lombok earthquakes, Indonesia, estimated through InSAR and GPS observations, *Nat. Hazards* 119,545–558, doi: 10.1007/s11069-023-06142-3.
- Gunawan, E., A. Gualandi, N. Rawlinson, S. Widiyantoro, M. Kholil, P. Supendi, G. H. Pramono, and S. T. Wibowo (2024). Complex fault system associated with the Molucca Sea Divergent double subduction zone revealed by the 2019 Mw 6.9 and Mw 7.1 earthquakes, *Tectonophysics* 230493, doi: 10.1016/j.tecto.2024.230493.
- Gunawan, E., N. R. Hanifa, D. H. Natawidjaja, T. Nishimura, S. Widiyantoro, B. Sugiarto, A. F. Shomim, and M. Ohzono (2024). Early postseismic slip of the 21 November 2022 Mw 5.6 Cianjur, Indonesia, earthquake based on GPS measurements, New Zeal. J. Geol. Geophys. doi: 10.1080/00288306.2024.2402254.
- Gunawan, E., W. Kongko, M. Kholil, B. T. Widyantoro, S. Widiyantoro, P. Supendi, N. R. Hanifa, I. M. Anjasmara, C. Pratama, and A. R. Gusman (2022). The 2019 Mw 7.0 Banten, Indonesia, intraslab earthquake: Investigation of the coseismic slip, tsunami modelling and Coulomb stress change, *Geoenviron*. Disast. 9, no. 14, doi: 10.1186/s40677-022-00215-4.
- Gunawan, E., T. Nishimura, S. Susilo, S. Widiyantoro, N. T. Puspito, D. P.
 Sahara, N. R. Hanifa, S. Hidayati, A. Omang, and A. Agustan (2020).
 Fault source investigation of the 6 December 2016 Mw 6.5 Pidie Jaya,
 Indonesia, earthquake based on GPS and its implications of the geological survey result, *J. Appl. Geodes.* 14, no. 4, 405–412.
- Gunawan, E., S. Widiyantoro, S. Rosalia, M. R. Daryono, I. Meilano, P. Supendi, T. Ito, T. Tabei, F. Kimata, Y. Ohta, and N. Ismail (2018).
 Coseismic slip distribution of the 2 July 2013 Mw 6.1 Aceh, Indonesia, earthquake and its tectonic implications, *Bull. Seismol. Soc. Am.* 108, no. 4, 1918–1928.
- Hardebeck, J. L., J. J. Nazareth, and E. Hauksson (1998). The static stress change triggering model: Constraints from two southern California aftershock sequences, J. Geophys. Res. 103, no. B10, 24,427–24,437.

- Herring, T. A., R. W. King, and S. C. McClusky (2010a). *GAMIT Reference Manual Release 10.4*, *Report*, Massachusetts Institute Technology, Cambridge, Massachusetts, 1–171.
- Herring, T. A., R. W. King, and S. C. McClusky (2010b). GLOBK Reference Manual: Global Kalman filter VLBI and GPS Analysis Program, Release 10.4, Report, Massachusetts Institute Technology, Cambridge, Massachusetts, 1–95.
- Hurukawa, N., B. R. Wulandari, and M. Kasahara (2014). Earthquake history of the Sumatran fault, Indonesia, since 1892, derived from relocation of large earthquakes, *Bull. Seismol. Soc. Am.* **104,** no. 4, 1750–1762.
- Irsyam, M., P. R. Cummins, M. Asrurifak, L. Faizal, D. H. Natawidjaja, S. Widiyantoro, I. Meilano, W. Triyoso, A. Rudiyanto, S. Hidayati, and M. Ridwan (2020). Development of the 2017 national seismic hazard maps of Indonesia, *Earthq. Spectra* **36**, no. 1_suppl, 112–136, doi: 10.1177/8755293020951206.
- Ito, T., E. Gunawan, F. Kimata, T. Tabei, M. Simons, I. Meilano, Agustan, Y. Ohta, I. Nurdin, and D. Sugiyanto (2012). Isolating along-strike variations in the depth extent of shallow creep and fault locking on the northern Great Sumatran Fault, *J. Geophys.* Res. 117, no. B6, doi: 10.1029/2011JB008940.
- King, G. C., R. S. Stein, and J. Lin (1994). Static stress changes and the triggering of earthquakes, *Bull. Seismol. Soc. Am.* **84**, no. 3, 935–953.
- Larson, K. M. (2019). Unanticipated uses of the global positioning system, Annu. Rev. Earth Planet. Sci. 47, no. 1, 19–40.
- Lentas, K., C. G. Gkarlaouni, N. Kalligeris, and N. S. Melis (2022). The 30 October 2020, MW= 7.0, Samos earthquake: Aftershock relocation, slip model, Coulomb stress evolution and estimation of shaking, *Bull. Earthq. Eng.* 20, no. 2, 819–851.
- Li, M., S. Zhang, C. Zhang, and Y. Zhang (2015). Fault slip model of 2013 Lushan earthquake retrieved based on GPS coseismic displacements, J. Earth Sci. 26, 537–547.
- Lin, J., and R. S. Stein (2004). Stress triggering in thrust and subduction earthquakes and stress interaction between the southern San Andreas and nearby thrust and strike-slip faults, *J. Geophys. Res.* **109**, no. B2, doi: 10.1029/2003JB002607.
- Marliyani, G. I., J. R. Arrowsmith, and K. X. Whipple (2016). Characterization of slow slip rate faults in humid areas: Cimandiri fault zone, Indonesia, *J. Geophys. Res.* **121**, no. 12, 2287–2308.
- McCaffrey, R. (2009). The tectonic framework of the Sumatran subduction zone, *Annu. Rev. Earth Planet. Sci.* **37**, no. 1, 345–366.
- Meade, B. J., P. M. DeVries, J. Faller, F. Viegas, and M. Wattenberg (2017). What is better than Coulomb failure stress? A ranking of scalar static stress triggering mechanisms from 105 mainshockaftershock pairs, *Geophys. Res. Lett.* **44**, no. 22, 11–409.
- Murase, M., N. Matta, T. Ishiyama, C. H. Lin, W. Chen, J. Y. Yen, J. B. H. Shyu, J. Lin, Y. Nishikawa, I. C. Yen, and F. R. Widiatmoko (2025). Effects of the 2022 Mw 7.0 Chihshang earthquake on the shallow creeping of the Central Longitudinal Valley Fault in Eastern Taiwan: Insights from precise leveling measurements, *Seismol. Res. Lett.* **96**, no. 3, 1521–1531.
- Nishimura, T., M. Sato, and T. Sagiya (2014). Global Positioning System (GPS) and GPS-Acoustic observations: Insight into slip along the subduction zones around Japan, *Annu. Rev. Earth Planet. Sci.* 42, no. 1, 653–674.

- Okada, Y. (1992). Internal deformation due to shear and tensile faults in a half-space, *Bull. Seismol. Soc. Am.* **82**, no. 2, 1018–1040.
- Prawirodirdjo, L., Y. Bock, J. F. Genrich, S. S. O. Puntodewo, J. Rais, C. Subarya, and S. Sutisna (2000). One century of tectonic deformation along the Sumatran fault from triangulation and Global Positioning System surveys, *J. Geophys. Res.* 105, no. B12, 28,343–28,361.
- Salman, R., E. O. Lindsey, L. Feng, K. Bradley, S. Wei, T. Wang, M. R. Daryono, and E. M. Hill (2020). Structural controls on rupture extent of recent Sumatran Fault Zone earthquakes, Indonesia, *J. Geophys. Res.* 125, no. 2, e2019JB018101, doi: 10.1029/2019JB018101.
- Socquet, A., J. Hollingsworth, E. Pathier, and M. Bouchon (2019). Evidence of supershear during the 2018 magnitude 7.5 Palu earth-quake from space geodesy, *Nature Geosci.* 12, no. 3, 192–199.
- Supendi, P., N. Rawlinson, B. S. Prayitno, D. Sianipar, A. Simanjuntak, S. Widiyantoro, K. H. Palgunadi, A. Kurniawan, H. A. Shiddiqi, A. D. Nugraha, and D. P. Sahara (2023). A previously unidentified fault revealed by the February 25, 2022 (Mw 6.1) Pasaman earthquake, West Sumatra, Indonesia, *Phys. Earth Planet. In.* 334,106973, 10.1016/j.pepi.2022.106973.
- Tanaka, Y., Y. Ohta, and S. I. Miyazaki (2019). Real-time coseismic slip estimation via the GNSS carrier phase to fault slip approach: A case study of the 2016 Kumamoto earthquake, *Geophys. Res. Lett.* 46, no. 3, 1367–1374.
- Toda, S., and R. Stein (2003). Toggling of seismicity by the 1997 Kagoshima earthquake couplet: A demonstration of time-dependent stress transfer, *J. Geophys. Res.* 108, no. B12, doi: 10.1029/2003JB002527.
- Toda, S., J. Lin, and R. S. Stein (2011). Using the 2011 Mw 9.0 off the Pacific coast of Tohoku Earthquake to test the Coulomb stress

- triggering hypothesis and to calculate faults brought closer to failure, *Earth Planets Space* **63,**725–730.
- Toda, S., R. S. Stein, K. Richards-Dinger, and S. B. Bozkurt (2005). Forecasting the evolution of seismicity in southern California: Animations built on earthquake stress transfer, *J. Geophys. Res.* **110**, no. B5, doi: 10.1029/2004JB003415.
- Wang, K., Y. Hu, and J. He (2012). Deformation cycles of subduction earthquakes in a viscoelastic Earth, *Nature* 484, no. 7394, 327–332.
- Wells, D. L., and K. J. Coppersmith (1994). New empirical relationships among magnitude, rupture length, rupture width, rupture area, and surface displacement, *Bull. Seismol. Soc. Am.* **84**, no. 4, 974–1002.
- Wessel, P., J. F. Luis, L. A. Uieda, R. Scharroo, F. Wobbe, W. H. Smith, and D. Tian (2019). The generic mapping tools version 6, Geochem. Geophys. Geosys. 20, no. 11, 5556–5564.
- Wright, T. J. (2016). The earthquake deformation cycle, *Astron. Geophys.* **54**, no. 7, 4–20.
- Yabuki, T., and M. Matsu'ura (1992). Geodetic data inversion using a Bayesian information criterion for spatial distribution of fault slip, *Geophys. J. Int.* 109, no. 2, 363–375.
- Yoshida, S., T. Maeda, and N. Kato (2020). Earthquake triggering model based on normal-stress-dependent Nagata law: Application to the 2016 Mie offshore earthquake, *Earth Planets Space* 72, 1–13.
- Zhang, Y., H. Bao, Y. Aoki, and A. Hashima (2023). Integrated seismic source model of the 2021 M 7.1 Fukushima earthquake, *Geophys. J. Int.* 233, no. 1, 93–106.

Manuscript received 11 December 2024
Published online 10 October 2025